SERBIAN JOURNAL OF ELECTRICAL ENGINEERING
Vol. 20, No. 2, June 2023, 269-281
UDC: 621.313.32:519.673 **DOI: https://doi.org/10.2298/SJEE2302269P**

A Proposed Method to Rotordynamic Analysis of a High-speed Permanent Magnet Synchronous Machine by Retention Sleeve

Hossein Parivar[1], Ahmad Darabi[1]

Abstract: In this paper, the authors present a novel analytical model for rotordynamic analysis of a high-speed permanent magnet synchronous machine (HS-PMSM) with a retention sleeve. The proposed analytical model has a fast response, accurate results, and sample formulation, and is validated with the finite-element method (FEM). The obtained results show the proper accuracy of the proposed analytical solution approach. The significant results are: The analytical formulation model proposed for the rotordynamic analysis of the HS-PMSMs can accurately calculate the displacement and the stress of the solid cylinder of the rotor at any high speeds and temperature rises. Furthermore, the proposed analytical model is concerning the temperature changes in the rotor and ensures requirements in any temperature rising and high rotational speeds.

Keywords: High-speed permanent magnet synchronous machine (HS-PMSM), Rotordynamic analysis, Retention sleeve, Finite-element method (FEM), Rotor.

1 Introduction

In HS-PMSMs, rotordynamic problems are important, when the rotor faces by centrifugal forces. In fact, the permanent magnets (PMs) are not satisfy protected against mechanical stresses resulting from the high speeds. Hence, a protected scheme based on non-magnetic allay retention sleeves is proposed to protect the rotor of the HS-PMSMs [1]. HS-PMSMs concerning their high efficiency and low volume and size are the first choice in high-speed applications [2, 3]. So, the utilization of HS-PMSMs has increased rapidly [4 – 6], and multiple prototypes of the HS-PMSMs are presented, designed, and manufactured in various literature, academic activities, and real types [7 – 13]. The design limitations of the HS-PMSMs also is a subject that researchers are still exploring. Most articles concentrate only on electrical limitations. Whereas there are limitations that restrict the design of high-speed machines such as the electromagnetic, mechanical, and thermal limitations [14]. These limitations are various owing to the types of

[1]Department of Electrical Engineering, Shahrood University of Technology, Shahrood, Iran;
E-mails: hosseinparivar72@yahoo.com; darabi_ahmad@hotmail.com

HS-PMSM. By using the FEM, the mechanical analysis of the HS-PMSMs is accomplished, though it is not available as a complete model.

In this paper, an analytical model for the rotordynamic model of an HS-PMSM with a retention sleeve is presented. Following, the analytical problems are validated by corresponding FEM results [1 – 8]. The results show that the analytical model predicted accurately the stress and displacement of the rotor of the HS-PMSM at the rated rotational speed.

The rest of this paper is categorized into 4 sections. Section 2 is introduced the proposed rotordynamic model. The modeling, simulation, and comparison with FEM results of [1, 8] are presented in Section 3. Finally, Section 4 covers the conclusion.

2 Proposed Rotordynamic Analysis

Fig. 1 shows the structure of an HS-PMSM's rotor protected by a retention sleeve.

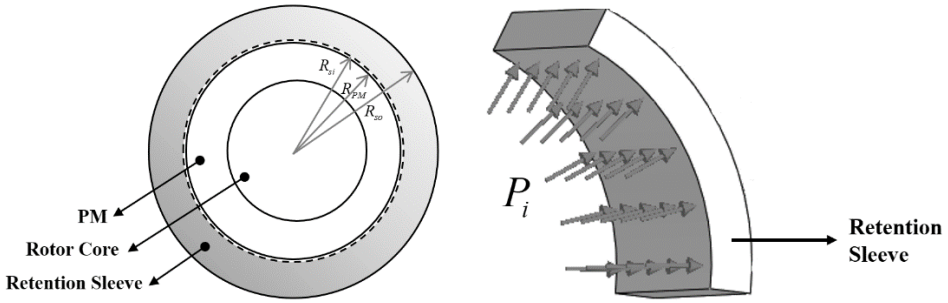

Fig. 1 – *Rotor structure of the HS-PMSM.*

The retention sleeve is a non-magnetic alloy and the PM of the rotor is a neodymium-iron-boron (NdFeB) which is modeled by a solid cylinder. In the first step, concerning Fig. 1 and define the inner radius of the retention sleeve (R_{si}), the outer radius of the retention sleeve (R_{so}), and the outer radius of the PM (R_{PM}), the shrink range (δ) is defined as (1):

$$\delta = R_{PM} - R_{si} . \tag{1}$$

The analytical formulation for the stress and displacement of the rotor is given by solving differential equations. Owing to Fig. 1, the contact pressure between PM and retention sleeve P_i is assumed by taking account of a relation between the radial displacements in the contact of the PM and the retention sleeve which are explained in the following sections. Concerning the theory of elastic mechanics, a differential equation such as (2) for the retention sleeve is produced

$$\frac{\mathrm{d}\sigma_{rs}}{\mathrm{d}r}+\frac{1}{r}\left(\sigma_{rs}-\sigma_{\theta s}\right)+\omega^2\rho_s r=0, \tag{2}$$

where σ_{rs} is the radial stress of the retention sleeve and $\sigma_{\theta s}$, ω and ρ_s are the tangential stress of the retention sleeve in the radius of *r*, angular velocity, and density, respectively. With consideration of a temperature rising in the retention sleeve and the radial displacement of the retention sleeve (u_s) in the radius of *r*, the group equation (3) is given

$$\begin{aligned}\varepsilon_{rs}&=\frac{\mathrm{d}u_s}{\mathrm{d}r}=\frac{1}{E_y}=\left(\sigma_{rs}-\mu_s\sigma_{\theta s}\right)+\alpha_h\Delta T_s,\\ \varepsilon_{\theta s}&=\frac{u_s}{r}=\frac{1}{E_y}=\left(\sigma_{\theta s}-\mu_s\sigma_{rs}\right)+\alpha_h\Delta T_s,\end{aligned} \tag{3}$$

where ε_{rs}, $\varepsilon_{\theta s}$, E_y, μ_s, and α_h are the radial strain and the tangential strain of the retention sleeve, Young modulus, Poisson ratio, and the thermal expansion coefficient of the retention sleeve of the rotor, respectively. $T_s(r)$ and $T_{s0}(r)$ are respectively defined as the temperature of the retention sleeve at the high-speed ratio and the temperature of the sleeve in the initial time which is equal to:

$$\Delta T_s=T_s(r)-T_{s0}(r), \tag{4}$$

with an expansions in (3), the group equation (5) is produced:

$$\begin{aligned}\sigma_{rs}&=\left[\frac{\mathrm{d}u_s}{\mathrm{d}r}+\mu_s\frac{u_s}{r}-(1+\mu_s)\alpha_h\Delta T_s\right]\frac{E_y}{1-\mu_s^2},\\ \sigma_{\theta s}&=\left[\frac{u_s}{r}+\mu_s\frac{\mathrm{d}u_s}{\mathrm{d}r}-(1+\mu_s)\alpha_h\Delta T_s\right]\frac{E_y}{1-\mu_s^2},\end{aligned} \tag{5}$$

with respect to (2) and (5), (6) is given:

$$\frac{\mathrm{d}^2u_s}{\mathrm{d}r^2}+\frac{1}{r}\frac{\mathrm{d}u_s}{\mathrm{d}r}-\frac{u_s}{r^2}=(1+\mu_s)\alpha_h\frac{\mathrm{d}\Delta T_s}{\mathrm{d}r}-\frac{\left(1-\mu_s^2\right)\rho_s\omega^2 r}{E_y}, \tag{6}$$

solving the aforementioned formula, (7) is produced:

$$u_s(r)=\Lambda_{1s}r+\frac{\Lambda_{2s}}{r}-\frac{(1-\mu_s^2)\rho_s\omega^2r^3}{8E_y}+\frac{1}{r}(1+\mu_s)\alpha_h\int_{R_{si}}^{r}\Delta T_s r\,\mathrm{d}r, \tag{7}$$

where Λ_{1s} and Λ_{2s} are two coefficients that are defined next. For the radial and tangential stress of the retentions sleeve, with substituting (7) in group (5), the group (8) is specified as:

$$\begin{aligned}\sigma_{rs}(r) &= -\frac{E_y\alpha_h}{r^2}\int_{R_{si}}^{r}\Delta T_s r\,\mathrm{d}r + \frac{E_y}{1-\mu_s^2}\left(\Lambda_{1s}\left(1+\mu_s\right)+\Lambda_{2s}\left(\mu_s-1\right)\frac{1}{r^2}\right)\\ &\quad -\frac{1}{8}\left(\rho_s\omega^2 r^2(\mu_s+3)\right),\\ \sigma_{\theta s}(r) &= \frac{E_y\alpha_h}{r^2}\int_{R_{si}}^{r}\Delta T_s r\,\mathrm{d}r - \frac{E_y}{1-\mu_s^2}\left(\Lambda_{1s}\left(1+\mu_s\right)+\Lambda_{2s}\left(1-\mu_s\right)\frac{1}{r^2}\right)\\ &\quad -\frac{1}{8}\left(\rho_s\omega^2 r^2(3\mu_s+1)\right).\end{aligned} \tag{8}$$

Both radial and tangential stress of the retention sleeve plays a role in the equivalent Von Mises stress of the retention sleeve. In this way, the equivalent of this parameter according to (8) is equal to:

$$\sigma_{eq1} = \left(\frac{1}{2}\left[\left(\sigma_{rs}-\sigma_{\theta s}\right)^2+\sigma_{rs}^2+\sigma_{\theta s}^2\right]\right)^{\frac{1}{2}}. \tag{9}$$

About the boundary condition of the retention sleeve which is defined as (10), two before mentioned coefficients Λ_{1s} and Λ_{2s} by $\zeta = R_{si}/R_{so}$ are as (11) and (12) respectively:

$$\begin{cases}\sigma_{rs}\big|_{r=R_{si}} = -P,\\ \sigma_{rs}\big|_{r=R_{so}} = 0,\end{cases} \tag{10}$$

$$\begin{aligned}\Lambda_{1s} &= \frac{-P(1-\mu_s)}{E_y(1-\zeta_s^{-2})} - \frac{(1-\mu_s)\alpha_h}{R_{si}^2(1-\zeta_s^{-2})}\int_{R_{si}}^{R_{so}}\Delta T_s r\,\mathrm{d}r\\ &\quad + \frac{\rho_s\omega^2 R_{so}^2(1-\mu_s)(3+\mu_s)(\zeta_s^2+1)}{8E_y},\end{aligned} \tag{11}$$

$$\begin{aligned}\Lambda_{2s} &= \frac{-P(1+\mu_s)R_{si}^2}{E_y(\zeta_s^2-1)} - \frac{(1+\mu_s)\alpha_h R_{si}^2}{R_{so}^2(\zeta_s^2-1)}\int_{R_{si}}^{R_{so}}\Delta T_s r\,\mathrm{d}r\\ &\quad + \frac{\rho_s\omega^2 R_{so}^2(1+\mu_s)(3+\mu_s)R_{si}^2}{8E_y}.\end{aligned} \tag{12}$$

According to Fig. 1, a compressive stress *P* acts on the outer surface of the PM. A differential equation for this part of the HS-PMSM for the radial displacement is determined as (13)

$$\frac{\mathrm{d}^2 u_{PM}}{\mathrm{d}r^2} + \frac{1}{r}\frac{\mathrm{d}u_{PM}}{\mathrm{d}r} - \frac{u_{PM}}{r^2} = -\frac{\rho_{PM}\omega^2 r}{E_{PM}}(1-\mu_{PM}^2) + \frac{\mathrm{d}\Delta T_{PM}}{\mathrm{d}r}\left[\alpha_{PM}(1+\mu_{PM})\right], \tag{13}$$

where u_{PM} is the radial displacements of the PM and ρ_{PM}, E_{PM}, μ_{PM} and α_{PM} are the density of the PM, Young modulus of the PM, Poisson ratio of the PM, and thermal expansion coefficient of the PM, respectively. Furthermore, both Λ_{1PM} and Λ_{2PM} coefficients can be determined next. The boundary condition of the PM is defined as (14), so Λ_{1PM} is as (15) and $\Lambda_{2PM}=0$:

$$u_{PM}\big|_{r=0}=0, \tag{14}$$

$$\Lambda_{1PM}=\frac{-P(1-\mu_{PM})}{E_{PM}}+\frac{(1-\mu_{PM})}{P_{oPM}}\alpha_{PM}\int_0^{R_{oPM}}\Delta T_{PM}\,r\,\mathrm{d}\,r + \frac{\rho_{PM}\omega^2 R_{oPM}^2\,(1-\mu_{PM})(3+\mu_{PM})}{8E_{PM}}, \tag{15}$$

$$\sigma_{rPM}(r)=-\frac{E_{PM}\alpha_{PM}}{r^2}\int_0^r\Delta T_{PM}\,r\,\mathrm{d}\,r + \frac{E_{PM}\Lambda_{1PM}(\mu_{PM}+1)}{1-\mu_{PM}^2}\frac{\rho_{PM}r^2\omega^2(\mu_{PM}+3)}{8}, \tag{16}$$

$$\sigma_{\theta PM}(r)=\frac{E_{PM}\alpha_{PM}}{r^2}\int_0^r\Delta T_{PM}\,r\,\mathrm{d}\,r+ \frac{E_{PM}\Lambda_{1PM}(\mu_{PM}+1)}{1-\mu_{PM}^2}\frac{\rho_{PM}r^2\omega^2(3\mu_{PM}+1)}{8}-\alpha_{PM}E_{PM}\Delta T_{PM}, \tag{17}$$

$$\sigma_{eq2}=\left(\frac{1}{2}\left[(\sigma_{rPM}-\sigma_{\theta PM})^2+\sigma_{rPM}^2+\sigma_{\theta PM}^2\right]\right)^{\frac{1}{2}}. \tag{18}$$

Also, the radial and the tangential stress of the PM can be calculated by (16) and (17), respectively so it is easy to obtain the equivalent Von-Mises stress of the PM as shown in (18). The sleeve prestress is calculated considering the compression of the PMs of the rotor at the calculated highest speed. As well, the thickness of the sleeve of the rotor is estimated to obtain a sufficient stress level at the same rated speed. So, the pressure loading imposed by the retention sleeve (p_{c_ps}) of the rotor is as (19):

$$p_{c\_ps}(r)=\sigma_{t\_ps}\left(\frac{r_i^2}{r_o^2-r_i^2}\left(1+\frac{r_o^2}{r^2}\right)\right)^{-1}, \tag{19}$$

where r_i and r_o are the inner radius and the outer radius of the sleeve, respectively and σ_{t_ps} is the prestress of the sleeve of the rotor and is calculated by (20):

$$\sigma_{t\_ps}=\frac{\Delta d}{2r_o}E_y, \tag{20}$$

where E_y and Δd are the sleeve Young Modulus and undersize, respectively.

3 Results

In this section, a 60 krpm, 40 kW, 2-pole, and 36 slots HS-PMSM with parameters (**Table 1**) and materials (**Table 2**) is modeled and designed in the first step. Also, the mechanical parameters of the PM and the sleeve of the rotor are summarized in **Table 3**. High-speed applications require PM materials with high operating temperatures and the ability to endure the mechanical stresses imposed by the high rotational speeds. NdFeB and samarium cobalt (SmCo) owing to their high energy density are preferred to use in these machines.

Table 1
HS-PMSM Design Parameters.

Parameters	Value	Parameters	Value
Stator Diameter in airgap side	77.00 mm	Stator wire diameter	1.43 mm
Efficient inner stator radius	38.54 mm	Stator outer diameter	133.26 mm
Stator core thickness	12.50 mm	Rotor core outer radius	34.50 mm
Rotor inner diameter	44.00 mm	Efficiency air gap	3.85 mm
Rotor radius in airgap side	37.50 mm	Slot area	165.00 mm^2
Physical airgap	1.00 mm	PM thickness	3.00 mm
Sleeve Thickness	3.85 mm	Stator core thickness	12.50 mm
Wire area	6.50 mm^2	Stator teeth width	3.11 mm

Table 2
HS-PMSM Materials.

Stator and Rotor Core	VACOFLUX-48
PM	NEOREC 50H (TDK)
Windings	Copper
Sleeve	Titanium

Table 3
Mechanical Properties of the Rotor.

	PM	Retention Sleeve
Mass Density	0.0075	0.0045
Young Modulus (MPa)	170000	120000
Poisson Ratio	0.24	0.34
Thermal Expansion Coefficient (10^{-6}/C)	4	9

VACOFLUX-48 is one of the well-known iron-cobalt alloys that is one of the most proper materials for utilization in HS-PMSM with a 30% higher saturation flux density compared to another alloy. To validate the proposed rotordynamic formulation to analyze the rotor of the HS-PMSM, the FEM model results are calculated in [1, 8], and compared with the proposed analytical model presented in this paper. The 60 krpm, 40 kW, 2-pole, and 36 slots HS-PMSM consists of four rotational parts named shaft, PMs, retention sleeve, rotor back-iron, and stator part with stator back-iron and 3-phase windings. To validate the proposed analytical method presented in this paper for the rotordynamic analysis, the stress components distribution of the PM rotor solid cylinder that is protected with a nonmagnetic alloy titanium retention sleeve is studied, analyzed, and compared with the FEM results according to [1, 8]. The following operation condition is selected for analyzing the stress component distribution of the PM and the retention sleeve:

– State I: The speed and temperature are constant i.e. $\Delta T_S - \Delta T_{PM} = 0$ or static state.

– State II: The speed at a high level of 60 krpm and temperature is constant: $\Delta T_S - \Delta T_{PM} = 0$.

– State III: The speed at a high level of 60 krpm and temperature rise: $\Delta T_S - \Delta T_{PM} = 120$.

Next, Figs. 2 – 4 are compared with the FEM results presented in [1, 8] and analytical formulae of stress components. The negative values are presented by compressive stress. In FEM analysis, a 2D model is used to calculate the stress component of the PM and the retention sleeve, and comparison with the analytical model. As shown in Figs. 2 – 4, the analytical method presented satisfactorily corresponds to FEM results presented in [1, 8].

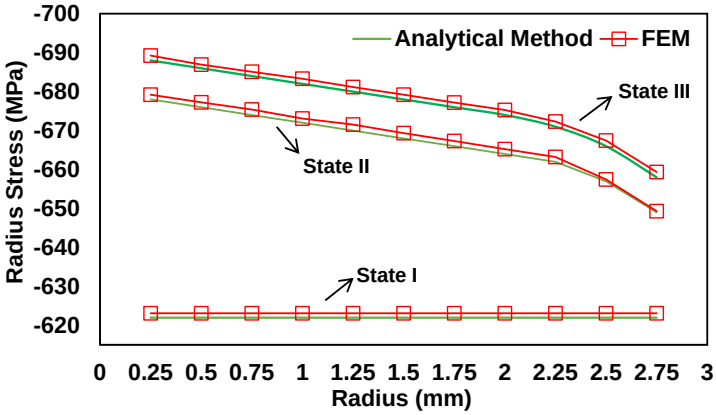

Fig. 2 – *Radial stress of the PM.*

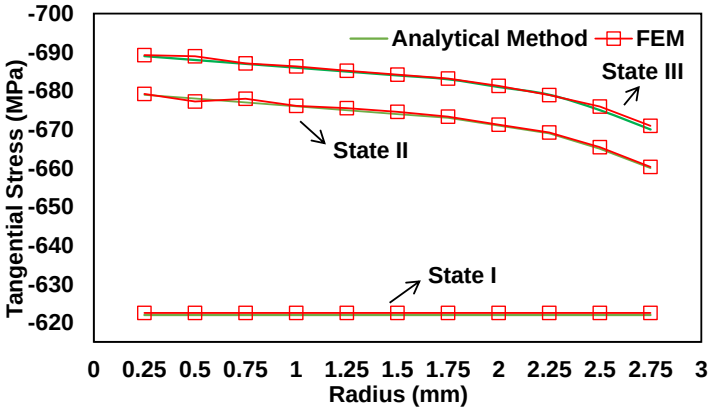

Fig. 3 – *Tangential stress of the PM.*

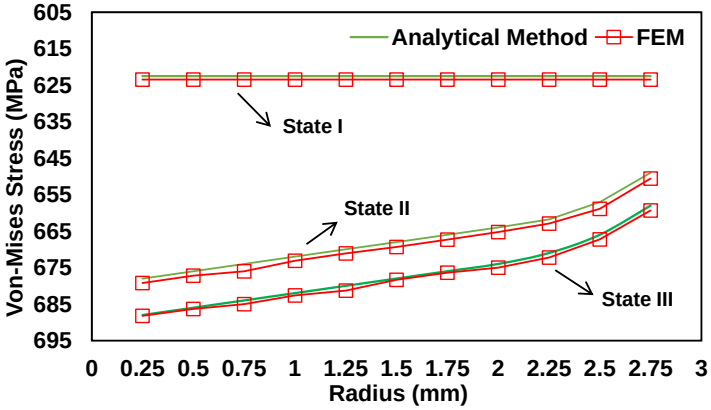

Fig. 4 – *Von-Mises stress of the PM.*

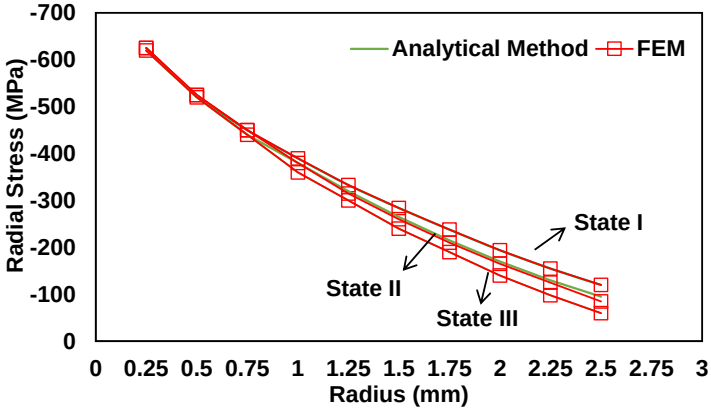

Fig. 5 – *Radial stress of the sleeve.*

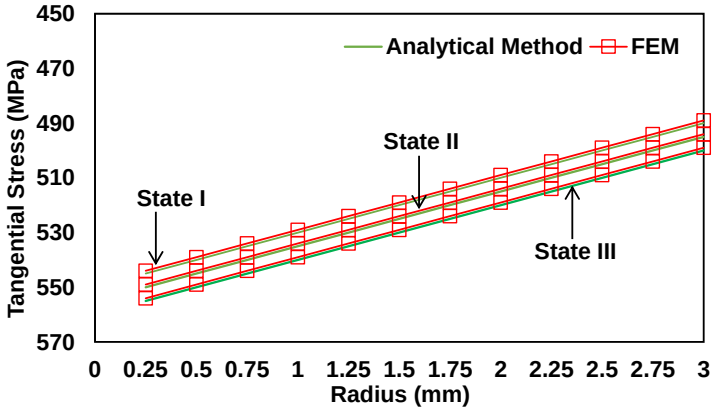

Fig. 6 – *Tangential stress of the sleeve.*

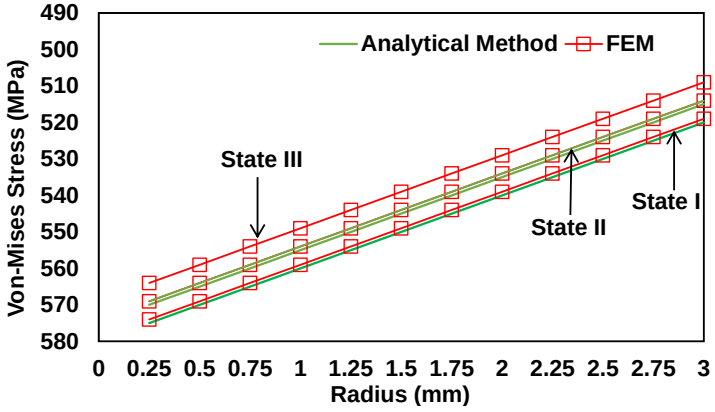

Fig. 7 – *Von-Mises stress of the sleeve.*

In State I (static state), the tangential stress, the radial stress, as well as the Von-Mises stress of the PM, is constant at about 621.3 MPa. In States II and III, the tangential stress, the radial stress, and the Von-Mises stress of the PM are increased during the radius direction of the PM. At the 60 krpm operation condition, the aforementioned stresses become less with respect to the centrifugal force of the PM. In State III and a temperature rise equal to $\Delta T_S - \Delta T_{PM} = 120$, the aforementioned stresses of the PM become future-reduced owing to a temperature rise in the rotor. As shown in Figs. 2 – 3, the radial and the tangential stress of the PM is negative in all operating States (State I to State III). It means that PM is in compression condition. Also, the corresponding stress components of the retention sleeve are indicated in Figs. 5 – 7 and verified the FEM results presented in [1, 8] with the presented analytical method. Fig. 5 shows the compressive state of the radial stress of the retention sleeve. Compared to the previous state, the radial stress gets less because of the effect of the centrifugal

force. In State III ($\Delta T_S - \Delta T_{PM}$ = 120), regarding increasing the heat in the rotor, the radial stress is reduced further. Fig. 6 also shows the centrifugal stress of the retention sleeve of the rotor. Compared to radial stress, it can result that the tangential stress of the retention sleeve is tensile. The FEM result results presented in [1, 8] and the analytical model results of the centrifugal stress and the Von Mises stress of the retention sleeve at the three states are illustrated in Figs. 6 and 7, respectively. The rotor's centrifugal force led to an increase in the centrifugal stress and the Von Mises stress of the retention sleeve, as well as the rise in the temperature of the rotor leads to a decrease in the stresses. Fig. 8 shows the variation of sleeve tangential prestress requirement with rotor radius (a) and sleeve undersize (b) to achieve the required prestress.

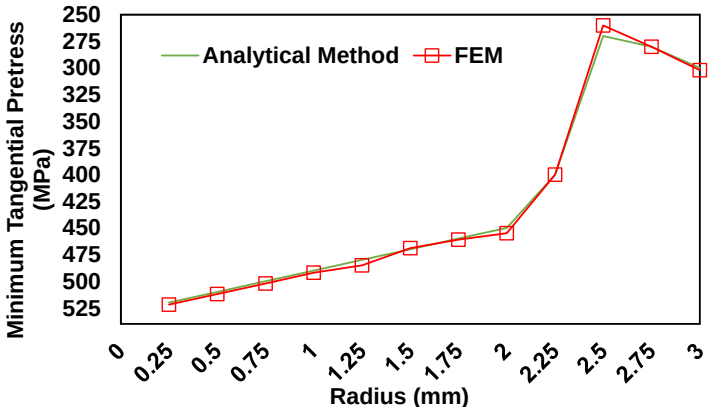

(a)

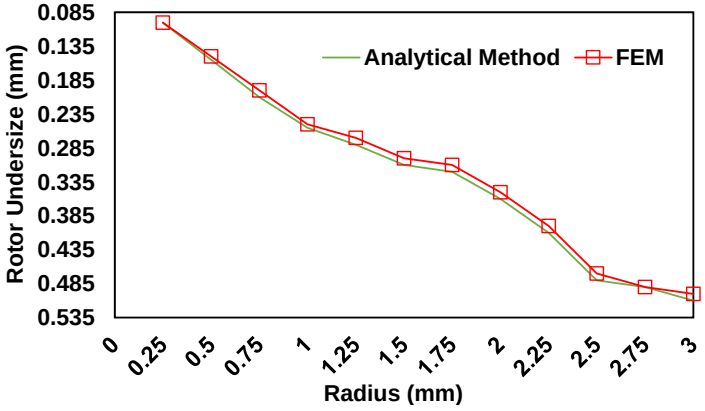

(b)

Fig. 8 – *The variation of sleeve minimum tangential prestress requirement with rotor radius* (a) *and sleeve undersize* (b) *to achieve the required prestress.*

As shown in Figs. 8a and 8b, the required prestress to achieve the PMs retention with a sleeve at the maximum speed of 60 krpm and the corresponding retention sleeve undersize to achieve the aforementioned prestress condition. The calculated Von Mises stress and Von Mises strain are illustrated in Fig. 9 through ABACUS FEM software. The obtained results show that for titanium material used in the retention sleeve, this value satisfies the operation condition of the designed 60 krpm, 40 kW, 2-pole, and 36 slots HS-PMSM, at rated 60 krpm rotational operation speed.

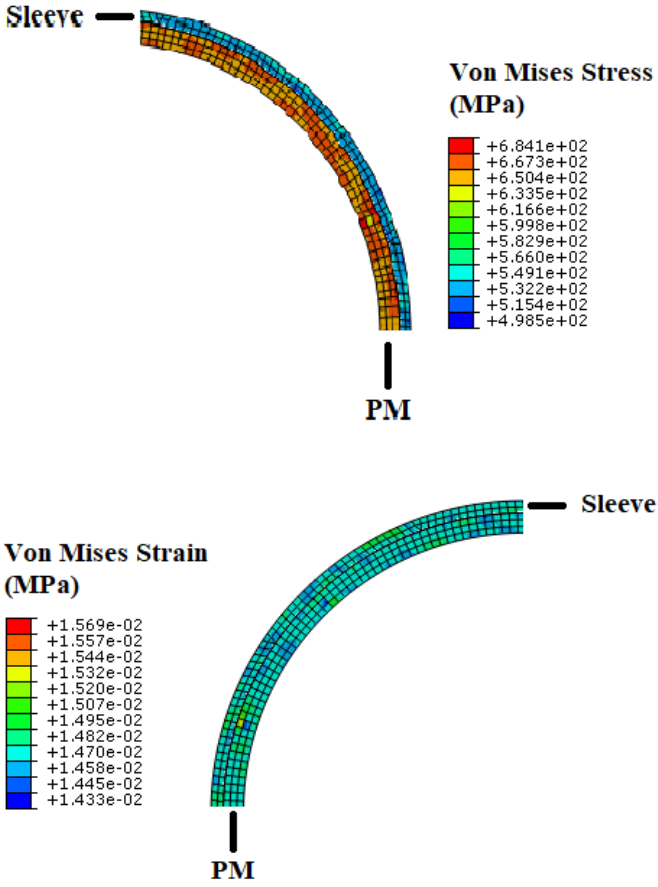

Fig. 9 – *Calculated Von-Mises stress and Von-Mises strain in rotordynamic analysis.*

4 Conclusion

In this paper, a novel analytical model for rotordynamic analysis of a 60 krpm, 40 kW, 2-pole, and 36 slots HS-PMSM is presented. This model has superiority with fast speed response, accurate results, and sample formula, and

validated with FEM results compared with other models ones presented in previous author's papers [1, 8].

The most significant obtained results are:

– The analytical formulation model proposed in this paper for rotordynamic analysis of the HS-PMSMs can accurately calculate the displacement and the stress of the solid cylinder of the rotor of the HS-PMSM, consisting of the PM and retention sleeve, at high speeds and any temperature rise, which in the previous papers, it is not considered.

– The temperature rises and parallels it, and the rotor heating problems and the centrifugal forces have significant effects on the rotor of the HS-PMSM rotordynamic analysis. Hence, the analytical model presented in this paper is presented with an eye to temperature changes in the rotor and ensures requirements in any temperature rising and high speeds.

The results obtained from this paper can potentially help the researchers, electrical machine designers, and manufacturing companies involved in high-speed machine analysis, modeling, design, and also optimization process.

5 Reference

[1] H. Parivar, A. Darabi: Taguchi Method for Design and Optimization of a High-Speed Permanent Magnet Synchronous Generator Protected by Retention Sleeve, Engineering and Applied Sciences, Vol. 7, No. 2, April 2022, pp. 21 – 28.

[2] M. Di Nardo, G. Gallicchio, M. Palmieri, A. Marfoli, M. Degano, C. Gerada, F. Cupertino: High-Speed Permanent Magnet Assisted Synchronous Reluctance Machine - Part II: Performance Boundaries, IEEE Transactions on Energy Conversion, Vol. 37, No. 4, December 2022, pp. 2567 – 2577.

[3] R. Wang, X. Fan, D. Li, R. Qu, Z. Liu, L. Li: Comparison of Heat Transfer Characteristics of the Hollow-Shaft Oil Cooling System for High-Speed Permanent Magnet Synchronous Machines, IEEE Transactions on Industry Applications, Vol. 58, No. 5, September-October 2022, pp. 6081 – 6092.

[4] Y. Yao, Y. Huang, F. Peng, J. Dong, Z. Zhu: A General Single-Sensor Damping Framework for LCL-Equipped High-Speed PMSM Drives, IEEE Transactions on Industrial Electronics, Vol. 70, No. 5, May 2023, pp. 5375 – 5380.

[5] H. Parivar, S. M. Seyyedbarzegar, A. Darabi: An Improvement on Slot Configuration Structure of a Low-Speed Surface-Mounted Permanent Magnet Synchronous Generator with a Wound Cable Winding, International Journal of Engineering, Vol. 34, No. 9, September 2021, pp. 2045 – 2052.

[6] H. Parivar, M. Shivaie, A. Darahi, M. Ansari: An Efficient Direct Torque Control Strategy for a Doubly Fed Induction Generator (DFIG) in Wind Energy Conversation Systems, Proceedings of the IEEE Texas Power and Energy Conference (TPEC), College Station, TX, USA, February 2021, pp. 1 – 5.

[7] A. H. Oguz, M. O. Gulbahce, D. A. Kocabas: Design and Optimization of an Axially-Slitted High-Speed Solid Rotor Induction Motor, Proceedings of the 9th International Conference on Electrical and Electronics Engineering (ELECO), Bursa, Turkey, November 2015, pp. 568 – 573.

[8] H. Parivar, A. Darabi: Design and Modeling of a High-Speed Permanent Magnet Synchronous Generator with a Retention Sleeve of Rotor, International Journal of Engineering, Vol. 34, No. 11, November 2021, pp. 2433 – 2441.

[9] H. Liu, L. Xu, M. Shangguan, W. N. Fu: Finite Element Analysis of 1 MW High Speed Wound-Rotor Synchronous Machine, IEEE Transactions on Magnetics, Vol. 48, No. 11, November 2012, pp. 4650 – 4653.

[10] M. Lafoz, P. Moreno-Torres, J. Torres, M. Blanco, G. Navarro: Design Methodology of a High Speed Switched Reluctance Generator Drive for Aircrafts, Proceedings of the 18th European Conference on Power Electronics and Applications (EPE'16 ECCE Europe), Karlsruhe, Germany, September 2016, pp. 1 – 9.

[11] G. W. Liu, G. W. Li, F. G. Zhang, S. Y. Yu: Design and Analysis of High Speed Outer Rotor Permanent Magnet Claw Pole Machine, Proceedings of the IEEE International Conference on Applied Superconductivity and Electromagnetic Devices (ASEMD), Shanghai, China, November 2015, pp. 230 – 231.

[12] X. Tian, Y. Xu, S. Wei: Design of a High-Speed Homopolar Inductor Machine for Flywheel Energy Storage System, Proceedings of the 22nd International Conference on Electrical Machines and Systems (ICEMS), Harbin, China, August 2019, pp. 1 – 5.

[13] M. Di Nardo, G. Lo Calzo, M. Galea, C. Gerada: Design Optimization of a High-Speed Synchronous Reluctance Machine, IEEE Transactions on Industry Applications, Vol. 54, No. 1, January-February 2018, pp. 233 – 243.

[14] G. Gallicchio, M. Di Nardo, M. Palmieri, A. Marfoli, M. Degano, C. Gerada, F. Cupertino: High-Speed Permanent Magnet Assisted Synchronous Reluctance Machines – Part I: A General Design Approach, IEEE Transactions on Energy Conversion, Vol. 37, No. 4, December 2022, pp. 2556 – 2566.